Monthly Notices
of the
ROYAL ASTRONOMICAL SOCIETY

MNRAS **488,** 4378–4388 (2019)
Advance Access publication 2019 July 25

doi:10.1093/mnras/stz2030

Relativistic Fe Kα line in the composite X-ray spectra of radio-loud active galactic nuclei

Jingwei Hu [1,2]★ Zhu Liu [1]★ Chichuan Jin[1] and Weimin Yuan[1,2]

[1]*Key Laboratory of Space Astronomy and Technology, National Astronomical Observatories, Chinese Academy of Sciences, Beijing, 100101, People's Republic of China*
[2]*School of Astronomy and Space Sciences, University of Chinese Academy of Sciences, 19A Yuquan Road, Beijing, 100049, People's Republic of China*

Accepted 2019 July 19. Received 2019 June 17; in original form 2019 January 17

ABSTRACT

While a broad Fe Kα emission line is generally found in the X-ray spectra of radio quiet (RQ) active galactic nuclei (AGNs), this feature, commonly thought to be broadened by the relativistic effects near the central black hole, appears to be rare in their radio loud (RL) counterparts. In this paper, we carry out a detailed study of the ensemble property of the X-ray spectra, focusing on the Fe line, of 97 RL AGNs by applying the spectral stacking method to the spectra obtained with *XMM–Newton*. For comparison, the same analysis is also performed for 193 RQ AGNs. Both a narrow and a broad component of the Fe Kα line are detected at high significance in the stacked spectra of both samples. The broad lines can be well fitted with relativistically broadened line profiles. Our results suggest that, as in their RQ counterparts, a relativistic Fe line component is commonly present in RL AGNs, though it may not be detected unambiguously in individual objects with spectra of relatively low signal to noise. We try to constrain the average spin of the black holes for both the RL and RQ AGN samples by modelling their composite Fe line spectral profiles with relativistic disc line models. For the RL sample, the average spin is loosely constrained and a wide range is allowed except for very fast spins (<0.78, 90 per cent confidence), while for the RQ sample, it is constrained to be low or moderate (<0.24). We conclude that the more precise measurement of the black hole spins in RL AGNs has to await for the advent of future high-throughput X-ray telescopes.

Key words: line: profiles – galaxies: active – galaxies: jets – X-rays: galaxies.

1 INTRODUCTION

The study of the radio properties of large samples of active galactic nuclei (AGNs) found that radio loud (RL) AGNs account for only 10–20 per cent of the whole population (e.g. Kellermann et al. 1989; Urry & Padovani 1995; Ivezić et al. 2002; Baloković et al. 2012). Observationally, the 'radio-loudness' parameter was applied to divide the AGN population into RL and RQ with the threshold $R_{5\,\mathrm{GHz}} = f_\nu(5\,\mathrm{GHz})/f_\nu(4400\text{Å}) = 10$, where $R_{5\,\mathrm{GHz}}$ is defined as the ratio between radio (5 GHz) and optical (B band) monochromatic luminosity (e.g. Kellermann et al. 1989; Stocke et al. 1992). However, the dichotomy in the radio-loudness distribution of quasars is still under debate (e.g. Cirasuolo et al. 2003).

The observed radio emission of RL AGNs is considered to originate from synchrotron emission from relativistic jets emanating from super massive black holes (SMBH) at the centre. These powerful jets carry substantial kinetic energy and deposit them into the surrounding medium, and such feedback could have profound impact on the evolution of the SMBH and their host galaxies (e.g. Fabian 2012). Yet it is still unclear how these relativistic jets are formed and powered (e.g. Blandford 2000; Meier 2003). Several theoretical models for the formation of jets have been proposed. One model is that the jet may be powered by energy extracted from a rapidly spinning black hole through the magnetic field anchored in the surrounding accretion disc (Blandford & Znajek 1977; Maraschi & Tavecchio 2003). It implies that AGNs with powerful jets should harbour a black hole (BH) with rapid spin (Czerny & You 2016). Alternatively, jets can be directly powered by accretion discs (Blandford & Payne 1982), in which case there appears no direct correlation between the presence of relativistic jets and the black hole spin. Therefore, the measurements of the spin distribution of black holes in RL and RQ AGN samples may give insight into the question as to how jets are formed.

The black hole spin measurement in AGNs is a rather difficult task (e.g. Strohmayer 2001; Brenneman & Reynolds 2006; Remillard & McClintock 2006; Broderick, Loeb & Reid 2011). A commonly used method is to infer the BH spin by modelling the broad Fe Kα line profile (Fabian & Miniutti 2005; Reynolds & Fabian 2008). Previously, two Fe Kα line components were often detected,

★ E-mail: hujingwei@nao.cas.cn (JH); liuzhu@nao.cas.cn (ZL)

including a narrow line and a broad line (e.g. Reynolds & Fabian 2008). The narrow Fe Kα line is believed to be produced by reprocessing of the X-ray emission from a central source by the dust torus which is far away from the black hole, and so its profile is barely affected by the relativistic effect of the strong gravitational field (Krolik & Kallman 1987; Nandra 2006). The broad Fe Kα line is often considered to originate from the innermost part of the accretion disc, with its asymmetric profile caused by the Doppler effect and gravitational redshift (Fabian et al. 1989, 2000). The line profile of the broad line depends on the inner radius of the accretion disc, which can extend to the innermost stable circular orbit (ISCO) whose size is determined by the black hole spin (Miller 2007). Theoretical calculation predicts a monotonic relation between the BH spin and ISCO (Bardeen, Press & Teukolsky 1972). Since the broadened of this line is highly dependent on the spin parameter of the black hole, it is possible to estimate the black hole spin by fitting the reflection spectrum [1] (Fabian & Miniutti 2005).

A broad component of the Fe Kα line has been detected in many RQ AGNs (Nandra et al. 1997, 2007; Patrick et al. 2012; Mantovani, Nandra & Ponti 2016). The BH spins of about two-dozen AGNs can be constrained from the broad line profiles (Brenneman 2013; Reynolds 2013). de La Calle Pérez et al. (2010) systematically analysed a sample of 149 RQ type-1 AGNs observed by *XMM–Newton*, and found that 36 per cent of the sources show strong evidence of a relativistic Fe Kα line with an average equivalent width (EW) of the order of 100 eV. This fraction can be interpreted as a lower limit in the wider AGN population. In RL AGNs, broad Fe lines and reflection humps are weak or absent. A possible explanation is that the reflection component is swamped by a beamed continuum (Fabian et al. 2000). However, it is still an open question as to whether a broad Fe line is commonly present in RL AGNs. Previous studies have reported the identification of a broad Fe Kα line in a small number of individual RL AGNs, such as 3C 111, 4C +74.26, 3C 120, 3C 390.3, 3C 445 (Lohfink et al. 2013, 2015). Among them very few sources have robust spin measurements. One example is 3C 120, in which a rapid BH spin is inferred $a > 0.95$ (Lohfink et al. 2013). A joint broad-band spectral analysis using *Suzaku*/*NuSTAR* observations of 3C 390.3 performed by Lohfink et al. (2015) suggested that the data were not good enough to constrain the black hole spin, although a large spin and very high emissivity can be derived from the spectral fitting with the reflection model.

However, the data quality of currently available observations of individual AGN was often too low to allow a detailed modelling of the broad Fe Kα line profile. By stacking the X-ray spectra of many AGNs, it is possible to improve the signal to noise (S/N) to study the ensemble property of the Fe line. Streblyanska et al. (2005) performed a stacking analysis on the *XMM–Newton* observations of the Lockmann Hole, finding broad relativistic Fe Kα lines with an EW of 560 and 460 eV for type 1 and type 2 AGNs, respectively. The strong red wing of this broad line feature suggests that the supermassive black holes may have on average high spin. Corral et al. (2008) developed a stacking method and applied it to a sample of type 1 AGNs. They detected a significant narrow Fe Kα emission line around 6.4 keV with an EW ∼90 eV, while no clear evidence of a broad relativistic emission line was found. Iwasawa et al. (2012) presented a spectral stacking analysis of ∼1000 X-ray sources with redshifts > 1 detected in the XMM-COSMOS field. They detected a broad Fe emission line at a low significant level (∼2σ) only in AGNs with low X-ray luminosities ($<3 \times 10^{44}$ erg s^{-1}) or intermediate Eddington ratios ($\lambda_{\rm Edd} \sim 0.1$). Chaudhary et al. (2012) concluded that the average Fe Kα line profile in their 248 AGNs sample from the 2XMM catalogue is best represented by a combination of a narrow and a broad line. A stacking analysis of 388 *XMM–Newton* spectra of a sample of 263 X-ray unabsorbed AGNs was performed by Falocco et al. (2014), and a relativistic Fe line was detected. By stacking the X-ray spectra of a sample of 51 narrow-line Seyfert 1 galaxies (NLS1s) observed with *XMM–Newton* using the method of Corral et al. (2008), Liu et al. (2015) found a broad Fe Kα line, and suggested that black holes in NLS1s may not spin very fast in general. By stacking the *XMM–Newton* spectra of a large, homogeneous sample of AGNs observed spectroscopically in the SDSS, Liu et al. (2016b) found that a broad Fe line is commonly present in type 1 AGNs, with its equivalent width increases with the Eddington ratio.

In this work, we examine the possible existence and the ensemble property of the Fe Kα line in the composite X-ray spectra of a sample of RL AGNs by stacking their *XMM–Newton* spectra using the method developed by Corral et al. (2008). The highly improved S/N of the composite spectra may reveal evidence for any possible broad line feature, which may hopefully shed light in the average spin of SMBH in RL AGNs in general. For comparison of the results of RQ AGNs, the same analysis is also performed for a sample of RQ AGNs.

This paper is organized as follows. In Section 2, we introduce the properties of the sample used in this work, with the detailed data processing procedures, including the stacking method used to obtain the composite spectra. In Section 3, we present our analysis of the stacked spectra for RL and RQ AGN samples. Finally, a discussion and conclusion about the implications from this work is presented in Section 4. Throughout this paper, we assume a flat cosmology with $\Omega_{\rm M} = 0.29$, $\Omega_{\Lambda} = 0.71$, and the Hubble constant $H_0 = 71$ km s^{-1} Mpc^{-1}.

2 SAMPLE SELECTION AND DATA REDUCTION

2.1 Sample Selection

Our original sample is selected from AGNs in the Véron-Cetty & Véron catalogue (Véron-Cetty & Véron 2010) which were observed with *XMM–Newton* observations included in the Third *XMM–Newton* Serendipitous Source Catalogue (Rosen et al. 2016). The VCV catalogue contains 133 336 quasars, 1374 BL Lac objects, and 34 231 active galaxies collected from the literature. It includes position and redshift information, as well as photometry (U, B, V) and 20 cm flux densities.

The 3XMM-DR6[2] catalogue contains 678 680 X-ray source detections drawn from 9160 *XMM–Newton* EPIC observations, covering an energy interval from 0.2 to 12 keV. These observations were made between 2000 February and 2015 June, and all the data sets have been publicly available. The median flux in the total energy band (0.2–12 keV) of the catalogue is 2.4×10^{-14} erg cm^{-2} s^{-1}; in the soft X-ray band (0.2–2 keV) the median flux is 5.7×10^{-15}

[1] However, there have been studies showing that the broad Fe Kα line can rise from the X-ray absorption of clumpy disc wind (Done & Jin 2016; Hagino et al. 2016).

[2] The production and content of the 3XMM catalogue are described in the 3XMM-DR6 User Guide at http://xmmssc.irap.omp.eu/Catalogue/3XMM-DR6/3XMM-DR6_Catalogue_User_Guide.html.

Table 1. Properties of the selected samples.

Parameters	RL	RQ	Total sample
Number of sources	97	193	290
Number of spectra	257	350	607
Redshift[a]	0.366	0.061	0.138
f_ν (5 GHz)[b]	0.037	0.002	0.006
f_ν (4400 Å)[c]	0.001	0.003	0.002
Flux[d]	1.4×10^{-12}	4.3×10^{-12}	2.7×10^{-12}
Luminosity[e]	4.9×10^{44}	0.4×10^{43}	1.2×10^{44}
Total counts[f]	1.7×10^{7}	2.4×10^{7}	4.1×10^{7}

Notes. [a]Median redshift; [b]median 5 GHz flux density in units of Jansky; [c]median 4400Å flux density in units of Janksy; [d]median 2–10 keV flux in units of erg cm^{-2} s^{-1}; [e]median 2–10 keV luminosity in units of erg s^{-1}; [f]the sum of 2–10 keV net photon counts.

erg cm^{-2} s^{-1}, and in the hard X-ray band (2–12 keV) it is 1.3×10^{-14} erg cm^{-2} s^{-1}. About 20 per cent of the sources in the catalogue have fluxes below 1×10^{-14} erg cm^{-2} s^{-1}.

We first select all the type-1 AGNs from the VCV catalogue, which consist of 19 696 sources. They are cross-matched with the 3XMM-DR6 catalogue with a radius of 5 arcsec. This results in a sample of 2243 type-1 AGNs with a total of 6929 X-ray observations. In order to estimate radio-loudness, objects without radio observations are discarded, while those covered by radio surveys are culled, including both detections and upper limits.

We select all the spectra taken with the EPIC-pn or EPIC-MOS cameras with more than 50 net counts in the 2–10 keV band for each of the detectors. Sources with substantial intrinsic column density $N_{\rm H} > 10^{22}$ cm^{-2}, as derived from spectral fitting, are also discarded. In the end, there are 290 type-1 AGNs with a total of 607 *XMM–Newton* observations. The median values of redshifts, 5 GHz flux density, 4400Å flux density and some other basic parameters of this sample are given in Table 1.

2.2 Samples of RL and RQ AGNs

The radio-loudness parameter $R_{5\,\rm GHz}$, adopted to classify AGNs into RL and RQ samples, is calculated as:

$$R_{5\,\rm GHz} = f_\nu(5\,\rm GHz)/f_\nu(4400\,\rm Å) \quad (1)$$

where f_ν(5 GHz) is the radio (5 GHz) flux density, f_ν(4400Å) is the optical (B band) flux density.

To compute the optical flux density $f_{\rm B}$, the Johnson B magnitude (Johnson & Morgan 1953) is calculated as (Véron-Cetty & Véron 2010):

$$B = M_B - 5 + 5 \times \log D + k - \triangle m(z) \quad (2)$$

where M_B is the B band absolute magnitude, D is the luminosity distance, k is the k-correction factor defined as $k = -2.5 \times log(1 + z)^{1-\alpha}$, z is the redshift, $\triangle m(z)$ is a correction to k correction in case that the spectrum of objects is not strictly follow the form $S \propto v^{-\alpha}$. The optical spectral index α (defined as $S \propto v^{-\alpha}$) is chosen to be 0.3 (Francis et al. 1991). The values of M_B, z and $\triangle m(z)$ for each sources are retrieved from the VCV catalogue. The B-band flux density f_B is calculated using the formula below:

$$f_B = 10^{-\frac{B_{\rm AB}+48.6}{2.5}} \quad (3)$$

where f_B is in units of erg s^{-1} Hz^{-1} cm^{-2}, $B_{\rm AB}$ is the B-band monochromatic AB magnitude (Oke & Gunn 1983), which can be converted from the commonly used UBVR colours, $B_{\rm AB} = B - 0.16$.

To improve the photometric accuracy, for those detected in the SDSS,[3] we adopt the SDSS optical magnitudes and compute f_B from the G and R magnitudes using formulas described in Véron-Cetty & Véron (2010). We only use the VCV magnitudes for those without SDSS detection. The rest-frame flux density at 6 cm (5 GHz) is determined from the observed flux density at 20 cm, assuming a power law with spectral slope $\alpha_\nu = -0.5$. Taking the k correction into account, we obtain the radio flux density in the rest frame. The radio-loudness parameter is calculated from equation (1), with the distribution shown in Fig. 1(a).

The objects are classified into two types, RL and RQ. The RL sample consists of 97 sources with $R > 10$. The RQ sample contains the remaining 193 sources, including 63 sources which are below the detection limits of existing radio surveys. Among the latter, 46 sources have upper limits on radio-loudness $R < 10$, and are thus radio quiet, whereas the remaining 17 sources have $R < 30$, in which case the classification is somewhat uncertain. Given that the upper limits are close to the dividing line of $R = 10$, we also consider these 17 sources to be mostly radio quiet in the following analysis. The distributions of the radio-loudness R, redshift, 2–10 keV net photon counts and intrinsic absorption column density $N_{\rm H}$ of the two samples are plotted in Fig. 1. The black solid and red dotted lines correspond to the RL and RQ AGN samples, respectively. It shows that although the redshifts of both samples span the 0–2.4 range, the majority (88 per cent) of the RQ AGNs lie below redshift 0.3, while the fraction of RL AGNs below this redshift is 47 per cent only. The median values for the parameters of the two samples are presented in Table 1.

2.3 Data processing

The X-ray observational ODF data are retrieved from the *XMM–Newton* Science Archive (XSA).[4] The data are reduced and analysed using the *XMM–Newton* Science Analysis Software (`SAS v 16.0.0`).[5] Following the `SAS` data analysis threads, the `epproc` (for EPIC-pn) and `emproc` (for EPIC-MOS) tasks are used to reprocess the data and generate new event lists. We filter the event lists to remove observational intervals during flaring particle background. X-ray spectra are extracted for the EPIC-pn and EPIC-MOS cameras. The source extraction region varies from source to source, but typically ranges between 15 and 30 arcsec. The background region, about 50 arcsec, is selected larger than the source extraction region. The redistribution matrix and ancillary file are obtained for each spectrum with the `SAS` tasks `rmfgen` and `arfgen`.

For bright sources the out-of-time events and pile-up effects are examined, which are found to be negligible for the extracted spectra. The MOS1 and MOS2 spectra of a given source are combined into one single EPIC-MOS spectrum using the `SAS` task `epicspeccombine`. All the spectra are rebinned using the FTOOLS task `grppha` so that each bin will have at least 25 counts. `XSPEC v12.9.1` is used to perform X-ray spectral analysis.

2.4 Stacking of X-ray spectra

In this work, we produce composite spectra for the RL and RQ AGN samples to achieve the highest possible S/N ratio, by stacking the

[3] http://skyserver.sdss.org/dr14/en/home.aspx
[4] http://nxsa.esac.esa.int
[5] https://www.cosmos.esa.int/web/XMM-Newton/sas-threads

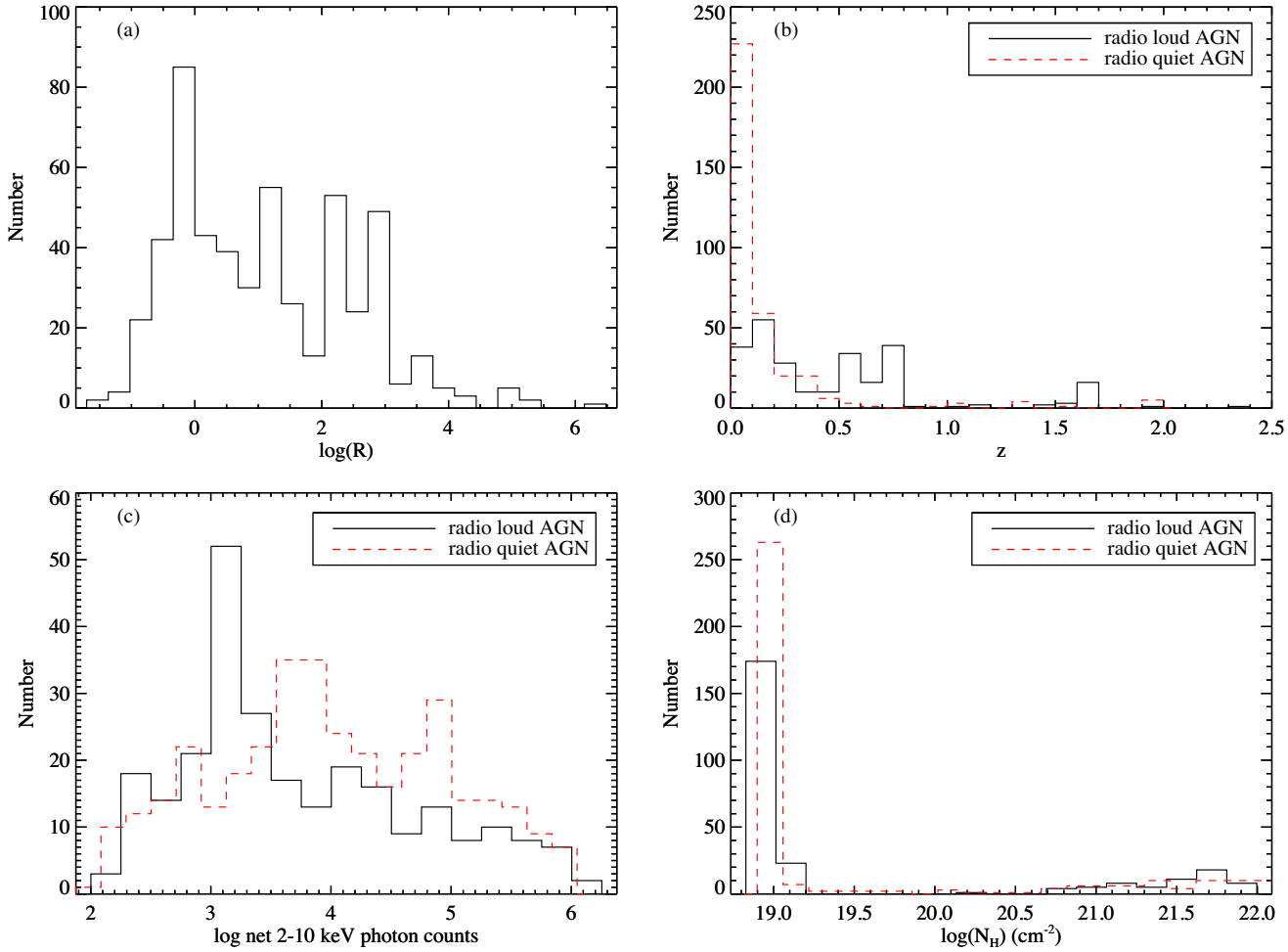

Figure 1. Panel a: Distribution of the radio-loudness of the sample objects. Panel b: Distribution of the redshift. The black solid and red dotted line correspond to the RL and RQ AGN samples, respectively. Panel c: Distribution of the 2–10 keV net photon counts. Panel d: Distribution of the intrinsic absorption column density.

individual spectra of the sample objects. To this end, we follow up on our previous series work (Liu et al. 2015, 2016a,b) and adopt the X-ray spectral stacking method developed by Corral et al. (2008). The details of the method can be found in Corral et al. (2008) and are briefly described in below (see also Falocco et al. 2012, 2013, 2014; Liu et al. 2015, 2016a,b).

(1) Obtaining the best-fitting continuum for individual sources

The first step is to obtain the best-fitting continuum for each of the objects in the sample. The data below 2 keV, in the source rest frame, are ignored because of the possible presence of the soft X-ray excess. The spectral data in the 6–7 keV range is also discarded to avoid any contribution from the Fe K lines. Then we fit the leftover spectra while a power-law model modified by Galactic and any possible intrinsic absorption (`phabs*zphabs*powerlaw` in `XSPEC`). The Galactic absorption column density $N_{\rm H\_gal}$ towards the line of sight of each of the source is taken from Kalberla et al. (2005) and fixed in the spectral fitting. The best-fitting values of the intrinsic absorption column density, the slope, and normalization of the power law are obtained.

(2) Unfolding the spectra of individual sources

Next, the unfolded spectrum of the continuum for each of the sources, in the 2–10 keV band in the source rest frame is calculated (using the `XSPEC` command `eufspec`), from the best-fitting model of the continuum. The unfolded spectrum can be considered as a true source spectrum with the instrumental effects eliminated, under the assumption that the fitted model is a true description of the source spectrum.

(3) Rescaling and rebinning the spectra

The unfolded spectrum of each source is corrected for the absorption effect and transformed into the rest frame of the source. Each spectrum is then renormalized according to the flux of the best-fitting continuum. This is to ensure that each spectrum has the same weight in the co-addition of the sample spectra. In addition, all the spectra are rebinned according to the same new binning scheme with a bin size of 100 eV.

(4) Co-addition of the spectra

Finally, the unfolded and rescaled spectra of all the individual sources of the samples are co-added using the unweighted arithmetic average to produce a composite (stacked) spectrum. Such a spectrum represents the averaged ensemble property of the whole sample.

2.5 Emission line broadening effect in stacked spectra

It should be noted that a narrow spectral feature can be broadened in the spectral stacking, due to the instrumental effects in mainly the unfolding procedure (Falocco et al. 2012, 2013, 2014; Liu et al.

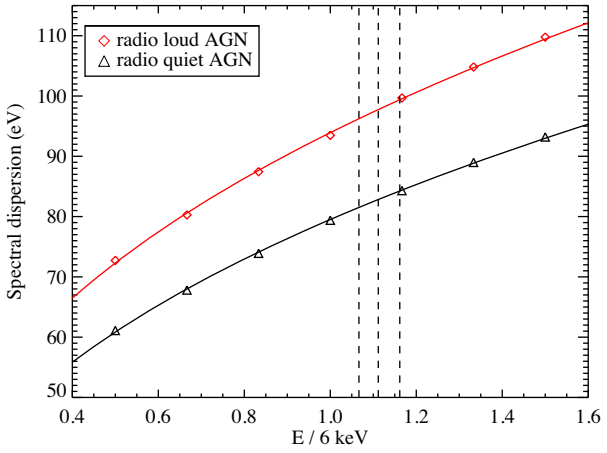

Figure 2. The broadening of the emission line due to the spectral stacking method at different energy in the source rest frame. The black dashed vertical lines mark the energies of the 6.4 (Fe I), 6.67 (Fe XXV) and 6.97 keV (Fe XXVI) emission lines. Trend of the spectral resolution $\Sigma(E)$ as a function of spectral energy E: $\Sigma(E) = 94\text{eV}(\frac{E}{6\text{keV}})^{0.38}$ for the RL AGN sample, $\Sigma(E) = 80\text{eV}(\frac{E}{6\text{keV}})^{0.39}$ for the RQ AGN sample.

2016a,b). We quantify the broadening effect by means of Monte Carlo simulations, in order to be able to take it into account in the spectral analysis at a later stage.

To do this, a Gaussian emission line with a width much narrower than the instrumental energy resolution is added in the best-fitting continuum model obtained for each of the objects. The line has a width $\sigma = 1$ eV, an equivalent width EW = 400 eV, and a line energy from 3 to 9 keV with a step of 1 keV. We simulate an 'observed' spectrum based on such a model for each of the sample objects using `fakeit` in `XSPEC`. We use an exposure 10 000 times longer than that in actual observation to achieve very high S/N in the simulated spectra. Then the same stacking method is applied to these simulated spectra, obtaining several stacked spectra in various centred line energies. A power-law continuum plus Gaussian line model is used to fit these spectra, finding that the input narrow line can be broadened increasingly with the higher input line energy.

The correlation between the line broadening and line energy is shown in Fig. 2. It can be well-described by a power-law function:

$$\Sigma(E) = \sigma_{6\text{keV}}(\frac{E}{6\text{keV}})^{\alpha} \quad (4)$$

where $\sigma_{6\text{keV}}$ represents Gaussian sigma at 6 keV, α represents power of energy for sigma variation, E represents the line energy and $\Sigma(E)$ represents the width of Gaussian smoothing at certain energy. The narrow Gaussian line at 6.4 keV appears to be broadened by $\Sigma(6.4\text{keV}) = 96$ eV for the RL sample and $\Sigma(6.4\text{keV}) = 82$ eV for the RQ sample. We apply the same simulation to different redshift subsamples, finding that the line can be more broadened for objects at higher redshift. So the spectral broadening is energy-dependent and redshift-dependent. To take this effect into account, we convolve the models with a Gaussian when fitting the stacked RL and RQ spectra.

3 THE STACKED COMPOSITE X-RAY SPECTRA

The stacked composite X-ray spectra are converted from the ASCII format to FITS file, by using the task `flx2xsp` in `FTOOLS` and are imported into `XSPEC` for modelling. Considering the spectral broadening effect introduced by the stacking method as discussed in Section 2.5 above, we convolve model spectra with a Gaussian using `gsmooth` in `XSPEC`. This procedure is applied to all spectral fits performed hereafter. The width of the Gaussian, which is energy dependent, is determined by equation (4), where the $\sigma_{6\text{keV}}$ and α parameters are estimated from simulations for various sample objects studied in the work. The rebinned spectra of the RL and RQ samples are shown in Fig. 3, and these errors are at the 1σ level. As in previous similar analysis, data below 3 keV are excluded due to the complexity of spectral components in this band (Corral et al. 2008; Liu et al. 2015). Data above 8 keV is also excluded for their low-S/N ratios. Thus, only the 3–8 keV band spectra are used for spectral analysis. First, the underlying continuum is fitted by ignoring the 5–7 keV range which contains potential contribution

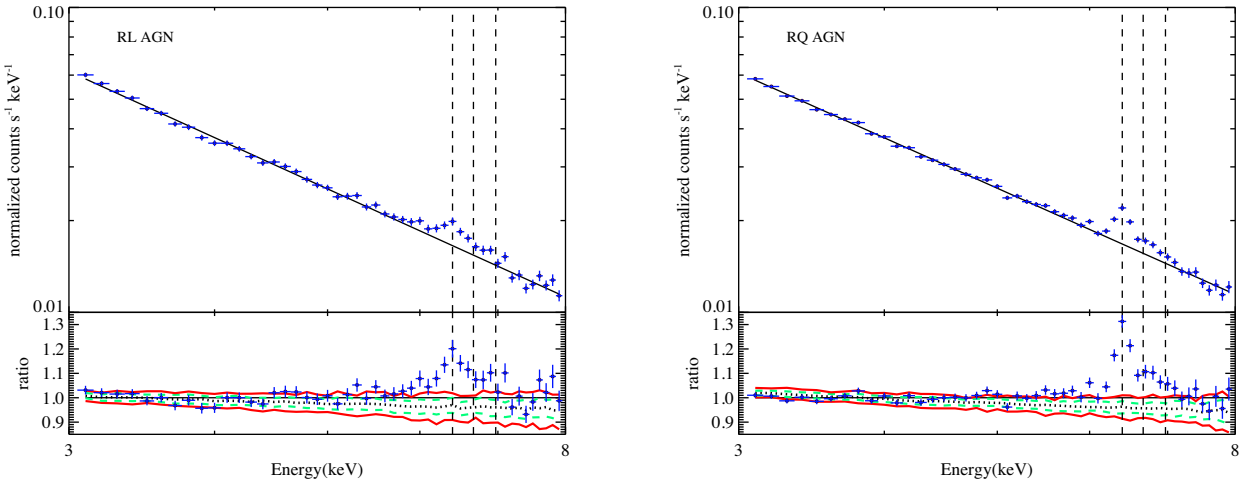

Figure 3. The composite spectra of both samples fitted with `powerlaw` model are shown in the upper plot of each panel. The underlying continuum is fitted by ignoring the 5–7 keV range which contains potential contribution from Fe K emission lines. The ratios of the stacked spectra to the model are shown in the lower plots of each panel. The black dotted line, the green dashed line and the red dot–dashed line represent the median, 1σ and 2σ continuum confidence lines of the simulations, respectively. The black dashed vertical lines mark the energies of the 6.4, 6.67, and 6.97 keV emission lines. Left-hand panel: the RL AGN sample. Right-hand panel: the RQ AGN sample.

Table 2. Spectral fits of the composite spectra with the gaussian model.

Model	Parameter							
	Γ	E (keV)	σ (eV)	EW (eV)	E (keV)	σ (eV)	EW (eV)	χ^2/d.o.f
(1)	(2)	(3)	(4)	(5)	(6)	(7)	(8)	(9)
				RL AGN sample				
PL+Narrow gau	1.70 ± 0.02	$6.45^{+0.01}_{-0.08}$	1(fixed)	50^{+13}_{-11}	–	–	–	69/45
PL+Narrow gau+narrow gau	1.71 ± 0.02	$6.75^{+0.07}_{-0.10}$	1(fixed)	22 ± 13	$6.35^{+0.09}_{-0.01}$	1(fixed)	49^{+11}_{-13}	60/43
PL+Gau	1.73 ± 0.03	6.42 ± 0.08	311^{+129}_{-107}	114^{+36}_{-32}	–	–	–	55/44
PL+Gau+narrow gau	$1.72^{+0.02}_{-0.03}$	6.67(fixed)	260^{+246}_{-158}	52^{+35}_{-32}	$6.35^{+0.10}_{-0.03}$	1(fixed)	37 ± 14	57/43
				RQ AGN sample				
PL+Narrow gau	1.67 ± 0.02	6.45 ± 0.01	1(fixed)	71 ± 9	–	–	–	72/45
PL+Narrow gau+narrow gau	1.69 ± 0.02	$6.75^{+0.05}_{-0.11}$	1(fixed)	27^{+7}_{-10}	$6.45^{+0.01}_{-0.07}$	1(fixed)	71 ± 9	49/43
PL+Gau	$1.68^{+0.01}_{-0.02}$	$6.42^{+0.01}_{-0.02}$	59^{+38}_{-48}	77^{+10}_{-12}	–	–	–	70/44
PL+Gau+narrow gau	$1.70^{+0.03}_{-0.02}$	$6.63^{+0.17}_{-0.13}$	300^{+193}_{-196}	64 ± 28	$6.40^{+0.01}_{-0.05}$	1(fixed)	50^{+12}_{-11}	46/42

Notes. For all the models, the spectral broadening effect resulting from the spectral stacking method adopted is taken into account by convolving the model with a Gaussian using the `gsmooth` model in `XSPEC`. The two parameters of `gsmooth`, the width of the broadening (σ_{6keV}) and the energy dependence index (α) are fixed at the values derived for these samples (see the text for details), i.e. $\sigma_{6keV} = 0.094$ and $\alpha = 0.38$ for the RL sample and $\sigma_{6keV} = 0.080$ and $\alpha = 0.39$ for the RQ one. The errors of the fitted parameters are at the 90% confidence level. The columns are: (1) spectral models. PL+Narrow gau: `gsmooth*(powerlaw+narrow gaussian)`; PL+Narrow gau+narrow gau: `gsmooth*(powerlaw+narrow gaussian+narrow gaussian)`; PL+Gau: `gsmooth*(powerlaw+gaussian)`; PL+Gau+narrow gau: `gsmooth*(powerlaw+gaussian+narrow gaussian)`; (2) photon index; (3)–(5) line energy, line width and equivalent width of the first Gaussian component; (6)–(8) line energy, line width and equivalent width of the second Gaussian component; (9) resulting chi-square and degrees of freedom.

from Fe K emission lines. For both the RL and RQ spectra, this underlying continuum can be well fitted with a power law. The best-fitting continuum (black solid line) as well as the data to model ratio (lower panels) are plotted in Fig. 3. A prominent spectral feature at around 6–7 keV is shown in the spectra as well as in the data to model ratio of both the RL and RQ spectra, which appears to be the Fe K emission lines.

To examine the reliability of these features, i.e. being statistically significant rather than fluctuations, we simulate the 'observed' X-ray spectra of the sample objects by assuming no Fe lines, and then perform the same stacking procedure. For each object of the samples, we simulate a source and a background spectra using `fakeit` by assuming the best-fitting continuum model found in Section 2.4 (step 1). The same exposure time, redistribution matrix and auxiliary file for each of the sources in our sample are used in these simulations to mimic the observed spectra. Such a procedure is repeated 100 times to produce 100 stacked simulated spectra for each sample. We can roughly estimate the 1σ (68 per cent) and 2σ (95 per cent) confidence intervals by calculating the 16–84th and 2–98th percentile values, respectively, in each energy bin, which are shown as the green dashed line and the red dot–dashed line in Fig. 3. The median of the simulated spectra is shown as the black dotted line. It is clear that the broad emission feature around 6.4 keV is detected significantly in the stacked spectra of RL and RQ AGN samples.

3.1 Modelling the stacked RL AGN spectra

We fit the composite spectra of the RL sample in the 3–8 keV band. We first add a narrow Gaussian line to the power law (`gsmooth*(powerlaw+narrow gaussian)`), which is commonly present in AGN spectra and is thought to be flourescence mission from a dusty torus. The line width is fixed at 1 eV. This model results in $\Gamma = 1.70 \pm 0.02$ with a poor reduced chi-square of $\chi^2/d.o.f = 69/45$, indicating that the model is unacceptable.

Next, we try to model the apparently broad feature with two narrow Gaussian lines (the widths fixed at 1 eV). The first line is fitted to have an energy of $E = 6.75^{+0.07}_{-0.10}$ keV and an equivalent width $EW = 22 \pm 13$ eV. While the second has $E = 6.35^{+0.09}_{-0.01}$ keV and $EW = 49^{+11}_{-13}$ eV. The fit is not acceptable with $\chi^2/d.o.f = 60/43$.

Then we try a model of one Gaussian line with the width as a free parameter. The fitted line energy is 6.42 ± 0.08 keV. The line width is 311^{+129}_{-107} eV, which is significantly larger than the artificial broadening of 96 eV due to the spectral stacking process for the RL AGN sample. The EW of line is 114^{+36}_{-32} eV. The reduced chi-square is $\chi^2/d.o.f = 55/44$. The improvement of the fit is significant, with $\Delta\chi^2 = 14$ for 1 additional degree of freedom ($P = 0.003$ using the F-test). Therefore, a broad line is a better description to the emission feature in the composite spectrum than the previous models with narrow lines.

We further add one more narrow Gaussian (line width fixed at 1 eV) to the broad line model, which is often seen in the X-ray spectra of AGNs. The narrow Gaussian line energy is $6.35^{+0.10}_{-0.03}$ keV. The broad line energy cannot be constrained, so we try to fix the line energy of the broad Gaussian component at 6.67 keV, similar to the line energy found in the double narrow-line model. However, there is no improvement of the fitting.

The results of the model fits are listed in Table 2. As can be seen, adding a broad Fe line improves the fit considerably over a pure power-law model, with a decrement in χ^2 of $\Delta\chi^2 = 63$ (a significant level $P = 8 \times 10^{-9}$ using the F-test). The fitting confirms that a broad Fe line is significantly detected in the composite spectrum of the RL sample.

The broadened Fe Kα line is believed to originate from the innermost part of the accretion disc, and its asymmetric profile arises from the Doppler and relativistic effects close to the black hole. This enables estimation of the black hole spin. For this purpose, the relativistic line model `relline` (Dauser et al. 2010) is adopted.

We try the relativistic line model `gsmooth*(powerlaw+relline+gaussian)` to fit the stacked RL spectrum. Several parameters are fixed at their

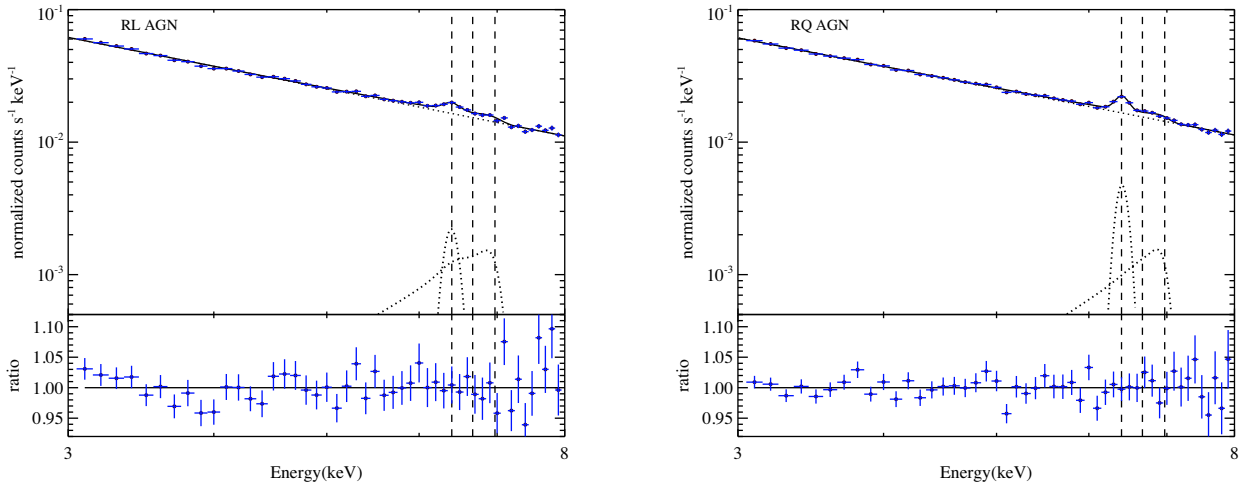

Figure 4. The composite X-ray spectra of both samples, with the best-fitting `gsmooth*(powerlaw+relline+gaussian)` model are shown in the upper plot of each panel. The data-to-model ratios are shown in the lower panel. Left-hand panel: For the RL AGN sample. Right-hand panel: For the RQ AGN sample.

Table 3. Spectral fits of the composite spectra with the relativistic Fe line and power-law continuum model.

Model	Parameter							
	Γ	E (keV)	Spin	EW (eV)	E (keV)	σ (eV)	EW (eV)	χ^2/d.o.f
(1)	(2)	(3)	(4)	(5)	(6)	(7)	(8)	(9)
				RL AGN sample				
PL+Relline+gau	1.75 ± 0.03	6.71 ± 0.13	<0.78	135^{+80}_{-69}	6.39 ± 0.05	1(fixed)	30 ± 12	48/42
				RQ AGN sample				
PL+Relline+gau	1.72 ± 0.02	$6.70^{+0.12}_{-0.10}$	<0.24	110^{+60}_{-52}	$6.41^{+0.01}_{-0.02}$	1(fixed)	55 ± 10	41/42

Notes. The same spectral broadening model gsmooth as in Table 2 is used (see caption of Table 2). The columns are: (1) spectral model. PL+Relline+gau: `gsmooth*(powerlaw+relline+gaussian)`; (2) photon index; (3)–(5) line energy, black hole spin, and equivalent width of the Relline component, the spin upper limits corresponding to the 90% confidence range; (6)–(8) line energy, line width, and equivalent width of the Gaussian component, we fix the line width as 1 eV when this value is derived close to 0; (9) resulting chi-square and degrees of freedom.

default values. The emissivity index is fixed at 3.0. We assume that the inner disc radius ($R_{\rm in}$) extends down to the ISCO, and fix the outer radius of the disc ($R_{\rm out}$) at 400 $r_{\rm g}$ ($r_{\rm g} = GM/c^2$ is the gravitational radius). The line energy in the rest frame of the disc and the spin of the black hole are both free parameters. We add a narrow Gaussian line component with a width fixed at 1 eV. However, the line energy and inclination angle in the `relline` model are highly degenerated and thus cannot be constrained well. Therefore, we fix $i = 30^{\circ}$ as the default value. The best-fitting model and the residual are shown in the left-hand panel of Fig. 4, and the parameters are listed in Table 3. This model can fit the data well, with $\chi^2/d.o.f = 48/42$ and an improvement of $\Delta\chi^2 = 22$. The equivalent width is 135^{+80}_{-69} eV for the `relline` component, and 30 ± 12 eV for the Gaussian component. The best-fitting line energy of the `relline` component is 6.71 ± 0.13 keV, corresponding to the ionized iron (Fe XXV). This implies that the line may originate from the inner disc that is highly ionized. However, the spin parameter cannot be well constrained. We examine the confidence region for the spin by finding the $\Delta\chi^2$ of the best fits with the change of spin by using `steppar` in `XSPEC`. The result is shown in Fig. 5. The average spin measured for the RL AGN sample is $a < 0.78$ at the 90 per cent confidence level.

To check if the spin parameter depends on the strength of the radio emission, we consider objects with radio-loudness greater than 100 only, which amount 162 objects. We stack the X-ray spectra for this subsample, and perform the same fitting procedure as above. A broad emission line is also significantly detected around 5–7 keV. The average spin for the $R_{\rm 5\,GHz} > 100$ subsample is $a < 0.75$ (at the 90 per cent confidence level) as shown in Fig. 5. Therefore, no dependence of the spin on the radio-loudness can be found from the current data.

The Fe line is expectedly accompanied by a reflection continuum, which has been ignored in the analysis above since its contribution to the X-ray spectrum below 8 keV is usually too small to have a considerable effect on the Fe line profile measurement. However, to make the analysis more self-consistent, we also take the reflection continuum into account in the modelling below. We first consider a reflection continuum from neutral material, i.e. `gsmooth*(powerlaw+relconv*pexmon+gaussian)` (Nandra et al. 2007). The abundance of iron is fixed at the solar value, while the photon index for an illuminating spectrum is linked to the value of the power-law continuum. The line width of the `gaussian` line is fixed at 1eV. However, this model results in a poor reduced chi-square of χ^2/d.o.f = 59/43, indicating that the model does not fit the spectrum well. The best-fitting line energy of the `relline` model suggests that the X-ray emission could arise from ionized material in the inner region of an accretion disc. So we consider a reflection continuum from ionized material, i.e.

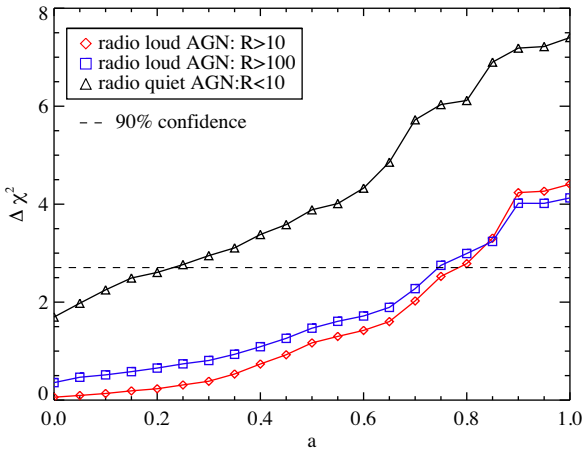

Figure 5. The $\Delta\chi^2$ of the fits with the change of the spin parameter, calculated using the `gsmooth*(powerlaw+relline+gaussian)` model. Red rhombus, blue square, and black triangle represent the spin of the R>10 RL AGN, R>100 RL AGN and R<10 RQ AGN samples, respectively. The black dashed horizontal line marks the 90 per cent confidence range of the black hole spin.

`gsmooth*(powerlaw+relconv*reflionx+gaussian)` (Ross & Fabian 2005). This model improves the fitting significantly over `pexmon` with χ^2/d.o.f = 47/42. The fitted parameters are broadly consistent with those of the `relline` model. The neutral narrow line is fitted with an energy of $E = 6.39 \pm 0.05$ keV and an equivalent width EW $= 29^{+16}_{-10}$ eV. The best-fitting ionization parameter is $\zeta = 384^{+1016}_{-176}$ erg cm s^{-1}, indicating an ionized reflector, consistent with the `relline` model. However, the average spin cannot be constrained for the RL AGN sample. The same is true for the `relxill` model (García et al. 2014) which combines reflection with relativistic broadening. Following the analysis of Falocco et al. (2014), we also consider the reprocessing by matter both far away from and close to the central black hole (`gsmooth*(powerlaw+relconv*reflionx+pexmon)`), but the model does not improve the fit and the additional parameters cannot be constrained.

3.2 Modelling the stacked RQ AGN spectra

For the RQ sample, we carry out the same fitting procedure as above for the RL one. We find the fitting results are similar to those for the RL sample, which are summarized below (see Figs 4, 5 and Tables 2, 3). A relativistic Fe line is significantly detected with a line energy $E = 6.70^{+0.12}_{-0.10}$ keV and an EW $= 110^{+60}_{-52}$ eV, consistent with previous results (Nandra et al. 2007; de La Calle Pérez et al. 2010; Patrick et al. 2012; Mantovani et al. 2016). A narrow line component is also found to be present at 6.4 keV, with EW $= 55 \pm 10$ eV. The averaged black hole spin is constrained to be $a < 0.24$ (at the 90 per cent confidence level, see Fig. 5). Similar to the RL sample, we also try to fit the average spectrum with a reflection continuum model (a neutral reflection model does not fit the spectrum well), i.e. `gsmooth*(powerlaw+relconv*reflionx+gaussian)`. This model can fit the data well, with χ^2/d.o.f. = 43/42. The energy and equivalent width of the narrow line are found to be $E = 6.41^{+0.01}_{-0.02}$ keV and EW $= 54^{+11}_{-9}$ eV, respectively. The best-fitting ionization parameter in the reflected model is $\zeta = 499^{+167}_{-242}$ erg cm s^{-1}. However, the average spin cannot be constrained well by using this reflected model.

4 DISCUSSION AND CONCLUSION

The broad Fe Kα line has been detected in some individual RL AGNs, such as 3C 111, 4C +74.26, 3C 120, 3C 390.3, 3C 445. Very few of them had spin measurement from the Fe Kα line. As shown in Lohfink et al. (2013), their preferred spectral solution for 3C 120 requires a large spin parameter of $a > 0.95$. A joint *Suzaku*/*NuSTAR* broad-band spectral analysis of 3C 390.3 performed by Lohfink et al. (2015) suggested that the data were not able to constrain the black hole spin, but high spin and high emissivity were implied by the reflection component. However, the number of sources with significant detection of broad Fe Kα line is still small, mainly because of the low data quality of individual sources. Thus, it is not clear whether the broad Fe Kα line is common in RL AGNs.

The stacking method used in this work can significantly improve the S/N ratio. A strong broad Fe line is significantly detected in the composite X-ray spectra of the RL and RQ sample. The broad lines can be well fitted by relativistically broadened Fe Kα line profiles, which are believed to be produced by reprocessing of the X-ray emission from the innermost part of the accretion disc. When fitted with the `relline` model, we find that the line energy is 6.71 ± 0.13 keV for the RL sample and $6.70^{+0.12}_{-0.10}$ keV for the RQ sample, consistent with ionized iron (Fe XXV). The EW of the broad line is found to be 135^{+80}_{-69} eV for the RL sample and 110^{+60}_{-52} eV for the RQ sample. This measurement is in good agreement with the EW of the order of 100 eV reported by de La Calle Pérez et al. (2010), where they found strong evidence of a relativistic Fe Kα line in 149 RQ type-1 AGN sample. It is also consistent with the result in Corral et al. (2008), who obtained an upper limit for the EW of 400 eV. A similar result was also found in Liu et al. (2015), with the EW of the broad line being 233 ± 113 eV and 400 ± 227 eV in the case of the additional narrow line being emission and absorption, respectively.

It should be noted that the BH spin of AGNs may be redshift-dependent (Berti & Volonteri 2008). As shown in Fig. 1, the redshift distributions of the RL and RQ samples are very different, with the RL AGNs extend to much higher redshifts than the RQ ones. Ideally, for a proper comparison the RL and RQ samples should have similar distributions in redshift and luminosity. As an attempt we try to select two subsamples (70 RL and 50 RQ objects) having similar redshift and luminosity distributions from the two parent samples, and produce two stacked composite X-ray spectra. However, the spectral S/N ratios are too low to give meaningful constraints to the broad Fe line profiles and thus the BH spins. Future larger samples with similar redshift and luminosity distributions are needed to eliminate the possible effect of redshift on the distributions of the BH spins, and even to test the evolution of the BH spins on redshift.

The average power-law photon index (when the reflection component is taken into account) of the RQ stacked spectrum ($\Gamma \sim 1.74$) is slightly flatter than the mean values found for typical RQ AGNs (1.9, Piconcelli et al. (2005)). We have examined this result by fitting the X-ray continuum spectra of the individual objects (with the Fe Kα line region filtered), and find that the average index is consistent with that derived from the composite spectrum. It has been suggested in previous studies that the X-ray spectral slopes of AGNs actually span a wide range, and are correlated with the Eddington ratio (e.g. Lu & Yu 1999; Shemmer et al. 2008). Therefore, the mean index depends on the statistical distribution of the Eddington ratio $\lambda_{\rm Edd}$. To examine this possibility, we cross-match our sample with the quasar catalogue of the SDSS DR7 quasars (Shen et al. 2011), resulting in a subsample of 63 sources with $\lambda_{\rm Edd}$ available. By dividing this subsample into different $\lambda_{\rm Edd}$ bins and evaluating the mean indices in each bin, we confirm a correlation between

Γ and $\lambda_{\rm Edd}$, which follows the relationship found for AGNs in previous studies (Shemmer et al. 2008). We therefore interpret the slightly flatter average spectral slope in the RQ sample results from its relatively lower Eddington ratio distribution compared to typical QSO samples. In fact, our sample comprises a large fraction of Seyfert galaxies, which have relatively lower Eddington ratios compared to luminous QSO.

Thanks to the large sample of AGNs analysed in this work, our results suggest that, as in their RQ counterparts, a broad Fe Kα line component is commonly present in RL AGNs, though it may not be detected unambiguously in individual objects with spectra of relatively low S/N. Furthermore, the measured EW of the broad Fe Kα line in the RL AGNs is in agreement with that in the RQ AGNs, suggesting that on average the strength of the broad Fe Kα line is comparable in RL and RQ AGNs. This may imply that the X-ray emission and interaction with surrounding matter in the RL AGNs is dominated by the corona-disc process that is similar to that in RQ AGNs.

Falocco et al. (2014) also studied the average X-ray spectrum of a sample of AGNs using a similar spectral stacking method. Our sample selection method is similar to theirs, i.e. AGNs in the VCV catalogue with *XMM–Newton* observations. However, comparing to our sample selection of type-1 RL and RQ AGNs in this work, the sources in their sample were classified as either AGNs or QSO. Both samples select unabsorbed AGNs ($N_{\rm H} < 10^{21.5}$ cm^{-2} in their sample and $N_{\rm H} < 10^{22}$ cm^{-2} in ours). In addition, their sample was defined by selecting spectra with S/N > 15, while we extract all the spectra with more than 50 net counts in the 2–10 keV band. In the study of Falocco et al. (2014), a disc-reflection component associated with the relativistic Fe line and a non-relativistic reprocessing component associated with the narrow Fe line were both detected significantly. The EWs of the relativistic and the non-relativistic line component were 72 ± 9 eV and 55 ± 7eV, respectively. Our spectral analysis are broadly in agreement with their results, e.g. the relativistic Fe line as well as the narrow Fe K line are significantly detected in both the RL and RQ subsample. The equivalent widths of the broad and narrow Fe K line components are also consistent with the Falocco et al. (2014) within uncertainty.

As predicted theoretically by Blandford & Znajek (1977), the jet in RL AGNs may be powered by energy extracted from a rapidly spinning black hole, i.e. the so-called Blandford–Znajek (BZ) mechanism. Using the BZ mechanism to calculate the jet power, Fanidakis et al. (2011) were able to reproduce the RL and RQ AGN populations. Some studies showed that central black holes in giant elliptical galaxies have tend to larger spins on average than black holes in spiral/disc galaxies, which can explain the AGN radio-loudness bimodality (e.g. Wilson & Colbert 1995; Volonteri, Sikora & Lasota 2007).

Observationally, whether or not the radio-loudness is correlated with BH spin is still controversial (e.g. Sikora, Stawarz & Lasota 2007; Chiaberge et al. 2015). The first direct evidence that jets in black hole binaries may be powered by black hole spin energy was presented by Narayan & McClintock (2012). However, no such evidence was found in another work using a different method (e.g. Fender, Gallo & Russell 2010). In addition, high spin BH can also be found in RQ AGNs (e.g. Wilms et al. 2001; Ghisellini, Haardt & Matt 2004).

In this work, we try to constrain the ensemble spin parameters of the black holes in both the RL and RQ AGN samples from the relativistic line profiles. As tentative results, the average spin is suggested to be $a < 0.78$ for RL AGNs ($R_{\rm 5\,GHz} > 10$) and $a < 0.24$ for RQ AGNs ($R_{\rm 5\,GHz} < 10$) at the 90 per cent confidence level in the `relline` model. For the $R_{\rm 5\,GHz} > 100$ RL AGN subsample, the broad Fe Kα line implies $a < 0.75$. Extremely large BH spin can be excluded at even the 99 per cent confidence level for our RQ AGNs. Thus, there is a hint that, on average, RL AGNs may have a wide spin distribution, while RQ have relatively low BH spins. However, we caution that these results can be considered only as suggestive given possible systematic uncertainties inherent in the spin measurement method, which are not well understood currently (e.g. Brenneman 2013). More precise measurements of the black hole spins of the AGN population have to await for the advent of future missions like *Athena* and *eXTP* with larger effective areas in the X-rays.

ACKNOWLEDGEMENTS

We thank our referee for his/her helpful comments and suggestions. This work is supported by the National Natural Science Foundation of China (grant no. 11873054, 11773037, 11673026, 11473035), thegravitational wave pilot B (grant no. XDB23040100), the Strategic Pioneer Program on Space Science, Chinese Academy of Sciences, grant no. XDA15310300, XDA15052100. This work is based on a recent observation conducted by *XMM–Newton*, an ESA science mission with instruments and contributions directly funded by ESA Member States and the USA (NASA).

REFERENCES

Baloković M., Smolčić V., Ivezić Ž., Zamorani G., Schinnerer E., Kelly B. C., 2012, ApJ, 759, 30
Bardeen J. M., Press W. H., Teukolsky S. A., 1972, ApJ, 178, 347
Berti E., Volonteri M., 2008, ApJ, 684, 822
Blandford R. D., 2000, R. Soc. London Trans. Ser. A, 358, 811
Blandford R. D., Payne D. G., 1982, MNRAS, 199, 883
Blandford R. D., Znajek R. L., 1977, MNRAS, 179, 433
Brenneman L., 2013, Measuring the Angular Momentum of Supermassive Black Holes. Springer-Verlag, Berlin
Brenneman L. W., Reynolds C. S., 2006, ApJ, 652, 1028
Broderick A. E., Loeb A., Reid M. J., 2011, ApJ, 735, 57
Chaudhary P., Brusa M., Hasinger G., Merloni A., Comastri A., Nandra K., 2012, A&A, 537, A6
Chiaberge M., Gilli R., Lotz J. M., Norman C., 2015, ApJ, 806, 147
Cirasuolo M., Celotti A., Magliocchetti M., Danese L., 2003, MNRAS, 346, 447
Corral A. et al., 2008, A&A, 492, 71
Czerny B., You B., 2016, Astron. Nachr., 337, 73
Dauser T., Wilms J., Reynolds C. S., Brenneman L. W., 2010, MNRAS, 409, 1534
de La Calle Pérez I. et al., 2010, A&A, 524, A50
Done C., Jin C., 2016, MNRAS, 460, 1716
Fabian A. C., 2012, ARA&A, 50, 455
Fabian A. C., Miniutti G., 2005, preprint (arXiv:astro-ph/0507409)
Fabian A. C., Rees M. J., Stella L., White N. E., 1989, MNRAS, 238, 729
Fabian A. C., Iwasawa K., Reynolds C. S., Young A. J., 2000, PASP, 112, 1145
Falocco S. et al., 2013, A&A, 555, A79
Falocco S., Carrera F. J., Corral A., Laird E., Nandra K., Barcons X., Page M. J., Digby-North J., 2012, A&A, 538, A83
Falocco S., Carrera F. J., Barcons X., Miniutti G., Corral A., 2014, A&A, 568, A15
Fanidakis N., Baugh C. M., Benson A. J., Bower R. G., Cole S., Done C., Frenk C. S., 2011, MNRAS, 410, 53
Fender R. P., Gallo E., Russell D., 2010, MNRAS, 406, 1425
Francis P. J., Hewett P. C., Foltz C. B., Chaffee F. H., Weymann R. J., Morris S. L., 1991, ApJ, 373, 465
García J. et al., 2014, ApJ, 782, 76
Ghisellini G., Haardt F., Matt G., 2004, A&A, 413, 535
Hagino K., Odaka H., Done C., Tomaru R., Watanabe S., Takahashi T., 2016, MNRAS, 461, 3954

Ivezić Ž. et al., 2002, AJ, 124, 2364
Iwasawa K. et al., 2012, A&A, 537, A86
Johnson H. L., Morgan W. W., 1953, ApJ, 117, 313
Kalberla P. M. W., Burton W. B., Hartmann D., Arnal E. M., Bajaja E., Morras R., Pöppel W. G. L., 2005, A&A, 440, 775
Kellermann K. I., Sramek R., Schmidt M., Shaffer D. B., Green R., 1989, AJ, 98, 1195
Krolik J. H., Kallman T. R., 1987, ApJ, 320, L5
Liu Z., Yuan W., Lu Y., Zhou X., 2015, MNRAS, 447, 517
Liu Z. et al., 2016a, MNRAS, 459, 1602
Liu Z., Yuan W., Lu Y., Carrera F. J., Falocco S., Dong X.-B., 2016b, MNRAS, 463, 684
Lohfink A. M. et al., 2013, ApJ, 772, 83
Lohfink A. M. et al., 2015, ApJ, 814, 24
Lu Y., Yu Q., 1999, ApJ, 526, L5
Mantovani G., Nandra K., Ponti G., 2016, MNRAS, 458, 4198
Maraschi L., Tavecchio F., 2003, ApJ, 593, 667
Meier D. L., 2003, New A Rev., 47, 667
Miller J. M., 2007, ARA&A, 45, 441
Nandra K., 2006, MNRAS, 368, L62
Nandra K., George I. M., Mushotzky R. F., Turner T. J., Yaqoob T., 1997, ApJ, 477, 602
Nandra K., O'Neill P. M., George I. M., Reeves J. N., 2007, MNRAS, 382, 194
Narayan R., McClintock J. E., 2012, MNRAS, 419, L69
Oke J. B., Gunn J. E., 1983, ApJ, 266, 713
Patrick A. R., Reeves J. N., Porquet D., Markowitz A. G., Braito V., Lobban A. P., 2012, MNRAS, 426, 2522
Piconcelli E., Jimenez-Bailón E., Guainazzi M., Schartel N., Rodríguez-Pascual P. M., Santos-Lleó M., 2005, A&A, 432, 15
Remillard R. A., McClintock J. E., 2006, ARA&A, 44, 49
Reynolds C. S., 2013, Class. Quantum Gravity, 30, 244004
Reynolds C. S., Fabian A. C., 2008, ApJ, 675, 1048
Rosen S. R. et al., 2016, A&A, 590, A1
Ross R. R., Fabian A. C., 2005, MNRAS, 358, 211
Shemmer O., Brandt W. N., Netzer H., Maiolino R., Kaspi S., 2008, ApJ, 682, 81
Shen Y. et al., 2011, ApJS, 194, 45
Sikora M., Stawarz Ł., Lasota J.-P., 2007, ApJ, 658, 815
Stocke J. T., Morris S. L., Weymann R. J., Foltz C. B., 1992, ApJ, 396, 487
Streblyanska A., Hasinger G., Finoguenov A., Barcons X., Mateos S., Fabian A. C., 2005, A&A, 432, 395
Strohmayer T. E., 2001, ApJ, 552, L49
Urry C. M., Padovani P., 1995, PASP, 107, 803
Véron-Cetty M.-P., Véron P., 2010, A&A, 518, A10
Volonteri M., Sikora M., Lasota J.-P., 2007, ApJ, 667, 704
Wilms J., Reynolds C. S., Begelman M. C., Reeves J., Molendi S., Staubert R., Kendziorra E., 2001, MNRAS, 328, L27
Wilson A. S., Colbert E. J. M., 1995, ApJ, 438, 62

APPENDIX A: SIMULATION FOR THE FE Kα EMISSION LINE

In this section, we carry out several simulations to roughly estimate the effect of different parameters in `gsmooth*(powerlaw+relline+gaussian)` model of both samples, shown in Figs A1 and A2. In case of different inclinations, we assume that the equivalent width is fixed at 0.2 keV and the fraction of sources with broad line is 100 per cent in the simulated spectra of both samples. The solid blue circles with error bars represent the ratio of the actual stacked spectrum to the simulated median continuum. The yellow short dashed line, green dot–dashed line and the red long dashed line represent the 1σ continuum confidence limits of the inclination 15°, 30°, 45°, respectively. In case of different equivalent widths, we assume that the inclination is fixed at 30° and the fraction of sources with broad line is 50 per cent in the simulated spectra of both samples. The yellow short dashed line, the green dot–dashed line and the red long dashed line represent the 1σ continuum confidence lines of the equivalent width 0.2, 0.3, 0.4 keV, respectively. A prominent spectral feature around 5–7 keV is shown in the simulated spectra. For both the RL and RQ AGN samples, the fraction of sources with a broad Fe Kα line should be much smaller than 100 per cent if the disc inclination is 15° and equivalent width is 0.2 keV.

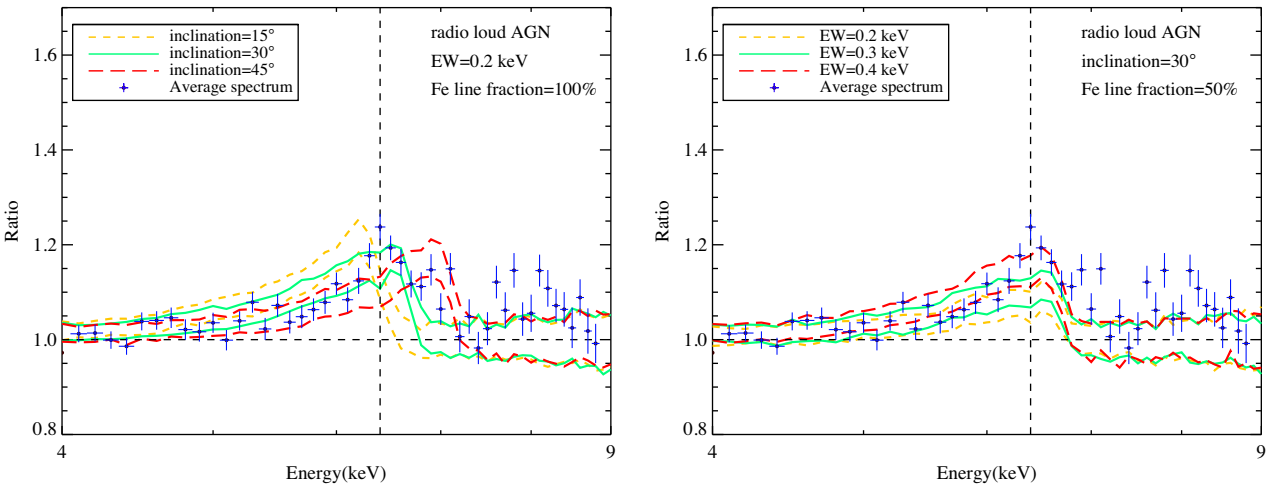

Figure A1. The simulated stacked X-ray spectra and the actual stacked spectrum for the RL AGN sample. The blue dots with error bars represent the ratio of the actual stacked spectrum to the simulated median continuum. Left-hand panel: The equivalent width is fixed at 0.2 keV and the fraction of sources with broad line is 100 per cent in the simulated spectra. The yellow short dashed line, the green dot–dashed line and the red long dashed line represent the 1σ continuum confidence lines of the inclination 15°, 30°, 45°, respectively. Right-hand panel: The inclination is fixed at 30° and the fraction of sources with broad line is 50 per cent in the simulated spectra. The yellow short dashed line, the green dot–dashed line and the red long dashed line represent the 1σ continuum confidence lines of the equivalent width 0.2, 0.3, 0.4 keV, respectively.

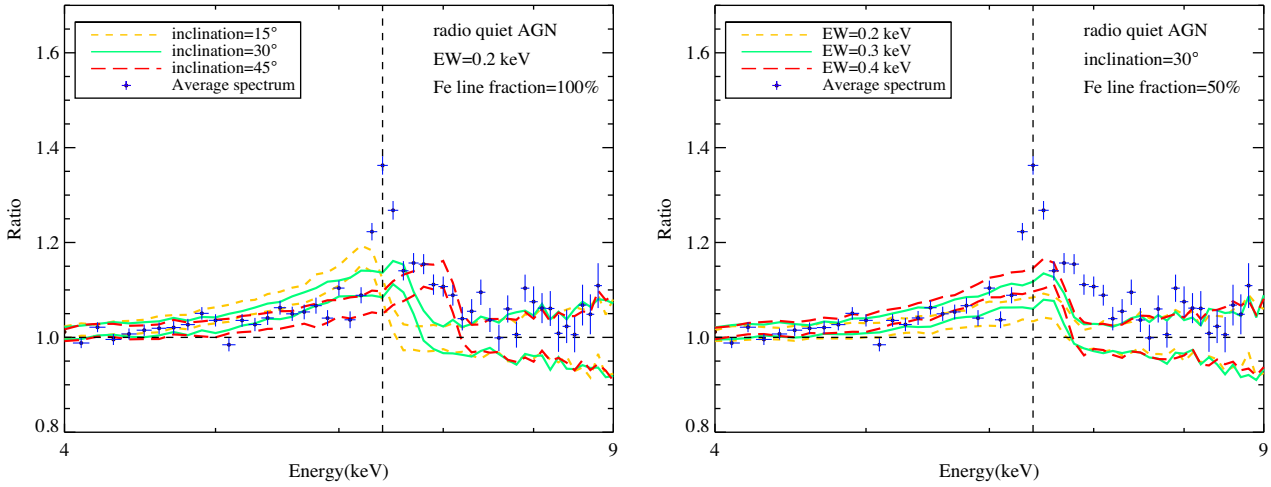

Figure A2. Same as Fig. A1, but for the RQ AGN sample.

This paper has been typeset from a TEX/LATEX file prepared by the author.